Materials Letters 264 (2020) 127372

Contents lists available at ScienceDirect

Materials Letters

journal homepage: www.elsevier.com/locate/mlblue

# Structure and mechanical properties of an *in situ* refractory $Al_{20}Cr_{10}Nb_{15}Ti_{20}V_{25}Zr_{10}$ high entropy alloy composite

N. Yurchenko [a,*], E. Panina [a], M. Tikhonovsky [b], G. Salishchev [a], S. Zherebtsov [a], N. Stepanov [a]

[a] Laboratory of Bulk Nanostructured Materials, Belgorod National Research University, Belgorod 308015, Russia
[b] National Science Center "Kharkov Institute of Physics and Technology" NAS of Ukraine, Kharkov 61108, Ukraine

ARTICLE INFO

*Article history:*
Received 22 October 2019
Received in revised form 14 January 2020
Accepted 16 January 2020
Available online 17 January 2020

*Keywords:*
Refractory high-entropy alloys
*In situ* composite
Structure
Thermo-Calc
Deformation behavior
Mechanical properties

ABSTRACT

Structure, deformation behavior, and mechanical properties of a refractory $Al_{20}Cr_{10}Nb_{15}Ti_{20}V_{25}Zr_{10}$ high entropy alloy are reported. In the as-cast state, the alloy had a composite-like hypoeutectic microstructure comprised of a softer primary B2 phase and a harder eutectic mixture consisting of a C14 Laves and the B2 phases. Annealing at 1200 °C retained the composite-like constitution and led to the formation of a small amount of a $Zr_5Al_3$-type phase. The annealing also had a positive effect on strength and ductility of the alloy at 22 and 800 °C; compatibility of plastic deformation at 800 °C can be ascribed to the relative softness of the B2 phase. Reasonable agreement was found between the experimental structures and the results of thermodynamic modeling.



## 1. Introduction

The recently introduced concept of refractory high entropy alloys (RHEAs) has illustrated a new way to develop metallic alloys with attractive high-temperature mechanical properties [1]. Some RHEAs demonstrate superiority over titanium aluminides and nickel-based superalloys in specific strength at T ≤ 1200 °C [2–4]. The ability to produce a superalloy-like bcc/B2 microstructure is considered promising for obtaining a balanced combination of properties [5,6]. However, many of the examined RHEAs contain different intermetallic phases, for example, the Laves phase, $Zr_xAl_y$, or $M_5Si_3$ [4,7–12]. Therefore, it is still unclear what type of microstructure is more suitable for the best properties obtaining [13].

An attractive option can be associated with the creation of an *in situ* composite consisting of two phases which possess substantially different hardness. For example, Laves phase-based alloys can have high strength at elevated temperatures but are brittle at ambient temperature [14]. One of the possible ways to attain better properties can be related to inserting a more ductile phase, like an ordered B2 one [15]. A eutectic B2 + Laves phase structure can, therefore, provide more tolerable toughness and improved high-temperature strength rather than the Laves phase or B2 intermetallics alone. However, there is minimal information on *in situ* RHEAs-based composites so far [9,11].

In this letter, we report the structure and mechanical properties of an $Al_{20}Cr_{10}Nb_{15}Ti_{20}V_{25}Zr_{10}$ high entropy alloy with a B2/Laves phase composite-like structure.

## 2. Materials and methods

The alloy with a nominal composition of $Al_{20}Cr_{10}Nb_{15}Ti_{20}V_{25}Zr_{10}$ was produced by vacuum arc melting of pure (≥99.9 wt%) elements. The actual chemical composition is given in Table 1.

The phase composition and microstructure of the alloy were studied for both the as-cast and annealed at 1200 °C for 24 h states using X-ray diffraction (XRD) and scanning electron microscopy (SEM). XRD analysis was performed using a RIGAKU diffractometer and Cu Kα radiation. Lattice strain was evaluated using the well-known Williamson-Hall method [16]. SEM investigations were performed on an FEI Quanta 600 FEG or a Nova NanoSEM 450 microscopes equipped with an energy-dispersive (EDS) and an electron backscattered diffraction (EBSD) detectors. The density of the alloy was measured via hydrostatic weighting. Compressive tests were performed using rectangular specimens measured 6 × 4 × 4 $mm^3$ on an Instron 300LX machine at 22 and 800 °C and the initial strain rate of $10^{-4}$ $s^{-1}$. The Scheil solidification path and equilibrium phase diagram were conducted using a Thermo-Calc 2019b software and TCHEA3 database.

* Corresponding author at: Laboratory of Bulk Nanostructured Materials, Belgorod National Research University, Pobeda 85, Belgorod 308015, Russia.
*E-mail address:* yurchenko_nikita@bsu.edu.ru (N. Yurchenko).

https://doi.org/10.1016/j.matlet.2020.127372
0167-577X/

**Table 1**
Chemical composition of the structural constituents of the $Al_{20}Cr_{10}Nb_{15}Ti_{20}V_{25}Zr_{10}$ alloy. The corresponding constituents are identified in Fig. 1b–e.

| Elements, at.% | Al | Cr | Nb | Ti | V | Zr | Microhardness, HV |
|---|---|---|---|---|---|---|---|
| Constituents designation | | | | | | | |
| Alloy composition | 21.3 | 9.7 | 12.7 | 18.7 | 27.2 | 10.4 | |
| Condition | As-cast | | | | | | |
| B2 phase | 17.8 | 9.0 | 15.3 | 20.6 | 33.5 | 3.8 | 665 ± 20 |
| Eutectic C14 Laves + B2 | 24.1 | 10.9 | 10.9 | 15.3 | 22.0 | 16.8 | 820 ± 30 |
| Condition | Annealed at 1200 °C, 24 h | | | | | | |
| B2 phase | 16.8 | 8.0 | 16.0 | 24.1 | 32.1 | 3.0 | 320 ± 25 |
| C14 Laves phase | 27.7 | 12.6 | 9.1 | 9.1 | 19.8 | 21.7 | 460 ± 40 |
| $Zr_5Al_3$-type phase | 35.7 | 1.3 | 11.7 | 12.3 | 6.3 | 32.7 | 600 ± 50 |

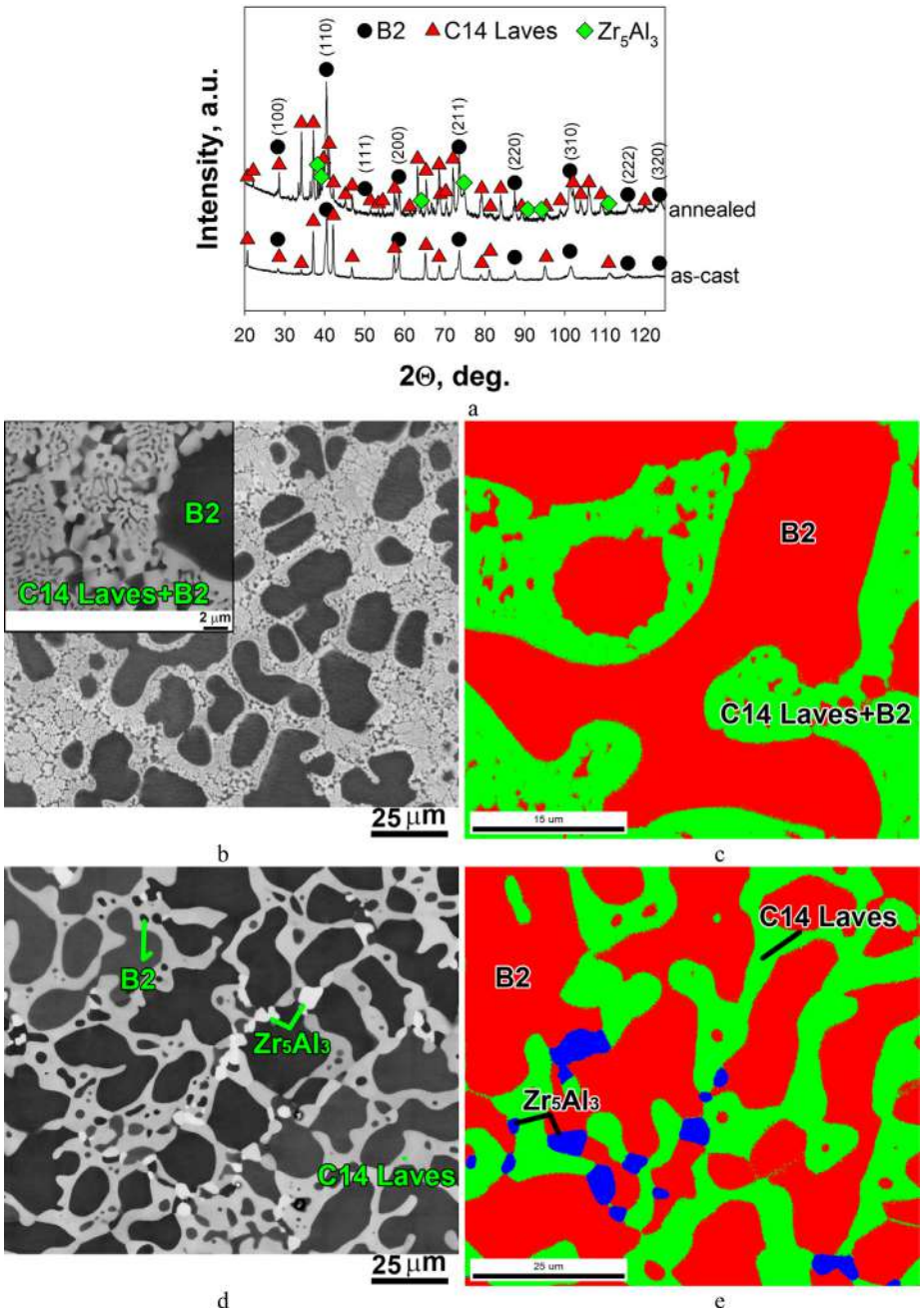


**Fig. 1.** XRD pattern (a) and microstructure of the as-cast (b, c) and annealed (d, e) $Al_{20}Cr_{10}Nb_{15}Ti_{20}V_{25}Zr_{10}$ alloy; b, d – SEM-BSE images; c, e – phase maps (red color – B2 phase, green – C14 Laves phase, blue – $Zr_5Al_3$-type phase). (For interpretation of the references to color in this figure legend, the reader is referred to the web version of this article.)

## 3. Results and discussion

According to XRD analysis (Fig. 1a), the as-cast $Al_{20}Cr_{10}Nb_{15}Ti_{20}V_{25}Zr_{10}$ alloy had a dual-phase structure presented by an ordered B2 phase and a C14 (hcp) Laves phase. Annealing led to the appearance of a new hexagonal $Zr_5Al_3$-type phase (Fig. 1a).

Combined SEM and EBSD analysis revealed that the as-cast RHEA possessed a microstructure comprised of the primary B2 phase, enriched with Nb, Ti, and V (Table 1), separated by eutectic (C14 Laves + B2) lamellar regions (Fig. 1b, c) enriched with Al, Cr, and Zr (Table 1). The volume fraction of the B2 and C14 Laves phases were 58% and 42%, respectively.

The annealed microstructure of the alloy inherited, in general, the composite-like constitution of the as-cast state (Fig. 1d, e). However, annealing resulted in (i) elimination of the lamellar structure and globularization/coalescence of the B2 phase in the eutectic C14 Laves + B2 regions and (ii) formation of the (Zr,Al)-rich particles ($Zr_5Al_3$-type phase) on B2/C14 Laves phase interfaces (Fig. 1c, d). The estimated volume fractions of the B2, C14 Laves, and $Zr_5Al_3$-type phases were found to be 61%, 36%, and 3%, respectively.

According to the Scheil-Gulliver model (Fig. 2a), the solidification of the RHEA started at ~ 1650 °C and terminated at ~ 1300 °C following the consequence L → L + bcc → L + bcc + C14 Laves. The equilibrium phase diagram predicted a narrow single-phase bcc region between 1560 and 1512 °C which then followed by the formation of the (Zr,Al,Cr)-rich C14 Laves phase (Fig. 3b). The C14 Laves phase fraction increased with a decrease in temperature till ~1100 °C and then remained almost constant (~0.31). Both the Scheil-Gulliver model and equilibrium phase diagram reasonably predict the type, chemical composition, and fraction of the C14 Laves phase. Also, the Scheil-Gulliver model accurately predicts the hypoeutectic morphology of the as-cast structure. Meanwhile, the B2 ordering and the $Zr_5Al_3$-type phase formation are not predicted, apparently due to the limitations of the existing databases [17].

Fig. 3 presents compressive stress–strain curves of the RHEA in the as-cast and annealed states. At 22 °C, the as-cast RHEA fractured in the elastic region at ~1000 MPa (Fig. 3a); meanwhile, the annealed RHEA demonstrated rather a high yield strength of 1535 MPa along with some ductility (ε = 0.6%, Fig. 3b). Microhardness measurements (Table 1) revealed the pronounced softening of both the B2 and C14 Laves phases after annealing. The lattice strain of the B2 phase in the as-cast state (ε = 0.1589) was ~2 times higher than that of annealed state (ε = 0.0852). This finding suggests the softening can be associated with internal stress relieving. The latter, along with globularization/coalescence of the B2 phase in the eutectic regions, can result in ductility improvement.

At 800 °C, stress–strain curves of the RHEA in both states had a pronounced softening stage after reaching peak stress. As a result of annealing, the yield strength of RHEA increased from 720 MPa to 1000 MPa. Partially this effect can be caused by the $Zr_5Al_3$-type phase formation [18]; however, a small fraction (3%) of this phase is hardly sufficient for such a substantial strength increment (~40%). Other factors, including changes in B2 ordering degree [8], can contribute to the high-temperature strength, but to establish their exact contribution, further investigations are needed. Nevertheless, the specific strength of the annealed RHEA was as high as 180 kPa*m$^3$/kg ($\rho$ = 5.55 ± 0.02 g/cm$^3$) indicating that it is one of the strongest RHEAs at 800 °C [1] most probably due to a composite-like structure with a continuous network of the hard Laves phase (Fig. 1).

To shed light on the deformation behavior of the $Al_{20}Cr_{10}Nb_{15}Ti_{20}V_{25}Zr_{10}$ alloy, microstructure in the annealed state after compression at 800 °C was analyzed. SEM images showed predominant localization of deformation in the softer B2 phase (Table 1, Fig. 3c, d), which ensures compatibility of plastic flow between phases and prevents propagation and coalescence of multiple microcracks formed in the C14 Laves and $Zr_5Al_3$-type phases. Since deformation at 800 °C does not result in the formation of visible grain/subgrain structure, the observed decrease in the flow stress at ε≈10% can rather be associated with intensive dynamic recovery rather than dynamic recrystallization. Tiny (150–300 nm) $Nb_2Al$-type particles (volume fraction ~ 2–3%) can be seen in the B2 phase after deformation at 800 °C; a similar effect was earlier observed in the $AlCr_{(0-0.5)}NbTiV$ alloys [4]. Generally, the deformation behavior of the $Al_{20}Cr_{10}Nb_{15}Ti_{20}V_{25}Zr_{10}$ alloy is very similar to that observed in the NbNiAl-NiAl alloys with a eutectic C14 Laves + B2 structure [15].

In summary, the presented data show that the $Al_{20}Cr_{10}Nb_{15}Ti_{20}V_{25}Zr_{10}$ RHEA can be considered as *in situ* composite consisting of the soft B2 and hard C14 Laves phases mixture (Fig. 1). After annealing, the alloy had some plastic ductility at 22 °C and high specific strength at 800 °C (Fig. 3). Besides, both experimental results and Thermo-Calc calculation (Figs. 1 and 2) suggested composite structure stability. Therefore, the $Al_{20}Cr_{10}Nb_{15}Ti_{20}V_{25}Zr_{10}$

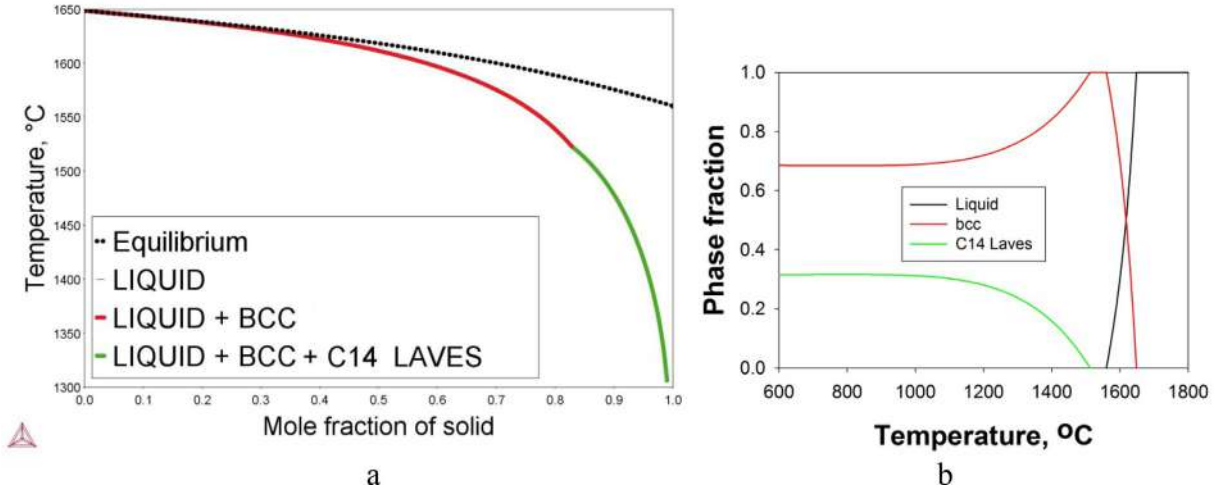


**Fig. 2.** Scheil solidification path (a) and equilibrium phase diagram (b) of the $Al_{20}Cr_{10}Nb_{15}Ti_{20}V_{25}Zr_{10}$ alloy.

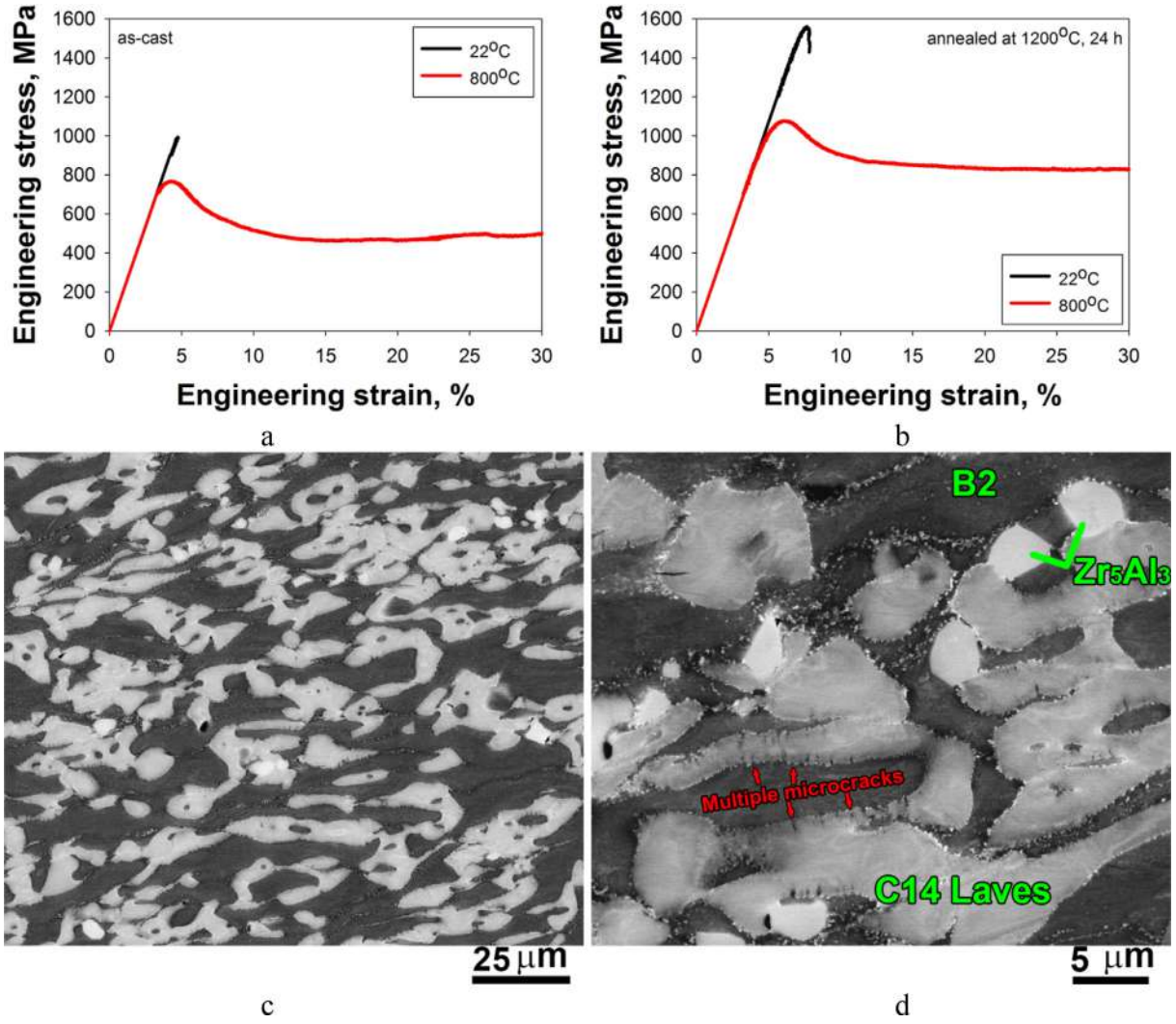


**Fig. 3.** Compressive stress–strain curves of the $Al_{20}Cr_{10}Nb_{15}Ti_{20}V_{25}Zr_{10}$ alloy (a, b) and microstructure of the specimen in the annealed state compressed at 800 °C to 50%; c, d – SEM-BSE images; the compression axis is vertical.

alloy, as well as other *in situ* RHEAs composites [9,11] can be considered as promising materials for high-temperature applications. However, further work is required to optimize the alloy's properties, including high-temperature strength, ductility, and oxidation resistance.

## 4. Conclusions

In this work, structure, deformation behavior, and mechanical properties of *in situ* refractory $Al_{20}Cr_{10}Nb_{15}Ti_{20}V_{25}Zr_{10}$ high entropy alloy composite was examined and the following conclusions were drawn.

1) In the as-cast state, the alloy had a hypoeutectic composite-like microstructure consisted of the primary B2 and C14 Laves + B2 eutectic regions. Annealing at 1200 °C led to the formation of a small amount $Zr_5Al_3$-type phase and globularization/coalescence of the B2 phase in the eutectic regions. Thermo-Calc reasonably predicted the solidification structure and its stability.
2) The alloy had limited ductility at 22 °C but became ductile at 800 °C. Annealing improved both strength and ductility of the alloy; the latter can be associated with increased plastic flow compatibility due to the softer B2 phase. The specific strength of the annealed alloy at 800 °C compared favorably with other RHEAs.

## CRediT authorship contribution statement

**N. Yurchenko:** Conceptualization, Methodology, Visualization, Formal analysis, Writing - original draft, Writing - review & editing. **E. Panina:** Investigation. **M. Tikhonovsky:** Resources. **G. Salishchev:** Project administration, Funding acquisition. **S. Zherebtsov:** Writing - review & editing. **N. Stepanov:** Supervision, Writing - review & editing.

## Declaration of Competing Interest

The authors declare that they have no known competing financial interests or personal relationships that could have appeared to influence the work reported in this paper.

## Acknowledgements

The authors gratefully acknowledge the financial support from the Russian Science Foundation Grant no. 19-79-30066. The

authors are grateful to the personnel of the Joint Research Center, “Technology and Materials”, Belgorod National Research University, for their assistance.

## Appendix A. Supplementary data

Supplementary data to this article can be found online at https://doi.org/10.1016/j.matlet.2020.127372.

## References

[1] O.N. Senkov, D.B. Miracle, K.J. Chaput, J.-P. Couzinie, J. Mater. Res. (2018) 1–37.
[2] O.N. Senkov, S.V. Senkova, D.B. Miracle, C. Woodward, Mater. Sci. Eng. A 565 (2013) 51–62.
[3] N.D. Stepanov, D.G. Shaysultanov, G.A. Salishchev, M.A. Tikhonovsky, Mater. Lett. 142 (2015) 153–155.
[4] N.D. Stepanov, N.Y. Yurchenko, D.V. Skibin, M.A. Tikhonovsky, G.A. Salishchev, J. Alloys Compd. 652 (2015) 266–280.
[5] V. Soni, O.N. Senkov, B. Gwalani, D.B. Miracle, R. Banerjee, Sci. Rep. (2018) 1–10.
[6] O.N. Senkov, J.K. Jensen, A.L. Pilchak, D.B. Miracle, H.L. Fraser, Mater. Des. 139 (2018) 498–511.
[7] O.N. Senkov, S.V. Senkova, C. Woodward, D.B. Miracle, Acta Mater. 61 (2013) 1545–1557.
[8] N.Y. Yurchenko, N.D. Stepanov, S.V. Zherebtsov, M.A. Tikhonovsky, G.A. Salishchev, Mater. Sci. Eng. A 704 (2017) 82–90.
[9] Y. Zhang, Y. Liu, Y. Li, X. Chen, H. Zhang, Mater. Lett. 174 (2016) 82–85.
[10] Y. Qiu, Y.J. Hu, A. Taylor, M.J. Styles, R.K.W. Marceau, A.V. Ceguerra, M.A. Gibson, Z.K. Liu, H.L. Fraser, N. Birbilis, Acta Mater. 123 (2017) 115–124.
[11] Y. Liu, Y. Zhang, H. Zhang, N. Wang, X. Chen, H. Zhang, Y. Li, J. Alloys Compd. 694 (2017) 869–876.
[12] Y. Cao, Y. Liu, Y. Li, B. Liu, J. Wang, M. Du, R. Liu, Mater. Lett. 246 (2019) 186–189.
[13] O.N. Senkov, S. Gorsse, D.B. Miracle, Acta Mater. 175 (2019) 394–405.
[14] A. Von Keitz, G. Sauthoff, Intermetallics 10 (2002) 497–510.
[15] L. Machon, G. Sauthoff, Intermetallics 4 (1996) 469–481.
[16] C. Suryanarayana, M.G. Norton, X-Ray Diffraction - A Practical Approach, Springer US, 1998.
[17] N.Y. Yurchenko, N.D. Stepanov, A.O. Gridneva, M.V. Mishunin, G.A. Salishchev, S.V. Zherebtsov, J. Alloys Compd. 757 (2018) 403–414.
[18] W. Chen, Q.H. Tang, H. Wang, Y.C. Xie, X.H. Yan, P.Q. Dai, Mater. Sci. Technol. (2018) 1–7.